Supporting Information

NiCoP@CoNi-LDH/SSM as multifunctional catalyst for high-efficient water splitting and ultra-long life rechargeable zinc-air battery

Juan Jian,[a,#] Zhuo Wang,[a,#] Yu Qiao,[a] Shuang Gao,[a] Meiting Wang,[a] Limin Chang,[a,*] Hairui Wang[a,*] and Ping Nie[a,*]

[a] Key Laboratory of Preparation and Applications of Environmental Friendly Material of the

Ministry of Education, College of Chemistry, Jilin Normal University, Changchun 130103, P. R.

China

*Corresponding authors' E-mails: changlimin2139@163.com; wanghairui9999@163.com;

xdnieping2009@sina.com

1. Material and Experimental Instruments

1.1 Materials used in the experiment

Pt/C (20 wt%) was obtained from Macklin Ltd. (Shanghai, China). RuO_2 was synthesized from ruthenium chloride hydrate ($RuCl_3 \cdot 3H_2O$) purchased from Beijing Chemical Reagents Company. (Beijing, China). Stain steel mash (SSM) was provided by the Hao Ke Technology Co. Ltd. (Beijing, China). KOH, $Co(NO_3)_2 \cdot 6H_2O$, $Ni(NO_3)_2 \cdot 6H_2O$, urea were supplied by the Beijing Chemical Reagents Company. NH_4F was purchased from Shanghai Titan Technology Co. Ltd. (Shanghai, China). NaH_2PO_2 was purchased from Shanghai Aladdin Biochemical Technology Co. Ltd. (Shanghai, China).

1.2 Experimental section

1.2.1 Preparation of the SSM

Immerse the 100 meshes SSM in HF acid solution for 10 minutes to achieve acid pickling and etching. Remove surface reactants from the etched stainless steel mesh by ultrasonic treatment in deionized water and anhydrous ethanol for 15 seconds. At last, dry the treated SSM at 60 °C vacuum for further use.

1.2.2 Preparation of the CoNi-LDH/SSM precursor.

First, dissolve 15 mmol $Co(NO_3)_2 \cdot 6H_2O$, 15 mmol $Ni(NO_3)_2 \cdot 6H_2O$, 170 mmol urea and 100 mmol ammonium fluoride (NH_4F) into 70 ml deionized water under magnetic stirring at room temperature to form a pink solution; then, place SSM (100 mesh, 304 L, 2 * 5 cm^2) into the pink solution and ultrasonic for 30 minutes; later, poured the above solution and SSM into a 100 ml Teflon-lined stainless-steel autoclave and maintained at 120 ℃ for 6 hours; last, washed the gained CoNi-LDH/SSM precursor with deionized water and anhydrous ethanol for several times, dried at 60 ℃ for 12 hours.

1.2.3 Preparation of NiCoP@CoNi-LDH/SSM, Pt/C/SSM, RuO_2/SSM and Pt/C+RuO_2/SSM.

Place the precursor at the downstream of a porcelain boat and the sodium hypophosphate at the upstream. Then, reacted at 300 ℃ for 2 hours under Ar atmosphere

and the final gained SSM based material is the NiCoP@CoNi-LDH/SSM, corresponding measured loading capacity is approximately 0.9 mg cm^{-2}. As for the comparison samples, we weighted the Pt/C and RuO$_2$ with the same loading capacity as the NiCoP@CoNi-LDH/SSM and gained the RuO$_2$/SSM (OER), Pt/C/SSM (HER, ORR) and Pt/C+RuO$_2$/SSM (air-cathode) as comparison samples. Wherein, the compared ink was consist of Pt/C (RuO$_2$), DMF, H$_2$O and Nafion ($V_{DMF}:V_{H2O}:V_{Nafion}$=4.5:4.5:1).

1.2.4 Basic phase characterizations

X-ray diffraction (XRD) experiment was tested on a Rigaku D-Max 2550 diffractometer with Cu-Kα radiation (λ = 1.5418 Å). Scanning electron microscope (SEM) and energy dispersive X-ray spectroscopy (EDX) images were obtained on a JEOL-6700 scanning electron microscope. Transmission electron microscope (TEM), high resolution TEM (HRTEM) images were obtained with microscopy of Philips-FEI Tecnai G2S-Twin, equipped with a field emission gun operating at 200 kV. X-ray photoelectron spectra (XPS) analysis was performed on a VG Scienta R3000 spectrometer with Al Kα (1486.6 eV) as the X-ray source. Contact angle (CA) experiment was analyzed by the machine of Dataphysics OCA20 at room temperature.

1.2.5 Electrochemical measurements

Electrochemical measurements were conducted using the three-electrode system with the electrochemical workstation (CHI 760e). The as-prepared electrodes were directly used as the work electrodes; meanwhile, graphite rod and Hg/HgO electrode were served as counter and reference electrodes, respectively. 1.0 M KOH solution was used as electrolyte for OER, while 0.1 M KOH solution was applied for ORR devices. Potentials were normalized versus the standard hydrogen electrode (RHE) according to formula below：

$$E_{(RHE)}=E_{(Hg/HgO)}+0.098 \text{ V}+0.591 \text{ pH}$$

Here, "$E_{(Hg/HgO)}$" was the potential we directly measured during the experiment. We applied the 1.0 M KOH throughout the OER and HER processes, thus, corresponding pH for OER and HER is 14; we applied the 0.1 M KOH for ORR, thus, the pH is 13 for ORR.

Polarization curves were performed via sweeping potentials at a scan rate of 0.5 mV s^{-1}. Corresponding stabilities were examined through current-time curves at the constant potentials.

Tafel slope

Tafel slope can be plotted by the gained linear sweep voltammetry (LSV) curves, which is obtained from the follow equation:

$$\eta = a + b \log j$$

Where, "η" refers to the overpotential; "j" is the current density; "a" relates to the j_0 (exchange current density) and can be reflected by the intercept; "b" is the Tafel slope we need to acquire.

Electrochemical active surface area (ECSA)

The ECSA was calculated by the formula below:

$$ECSA = A * C_{dl} / C_s$$

Here, "A" refers to the area of the working electrode, and we set the electrode area to 0.25 cm^2 throughout the electrocatalytic testing; "C_s" relates to the electrolyte and C_s = 0.04 mF cm^{-2}, "C_{dl}" is the abbreviation of double layer capacitance and calculated from a series of CV curves that tested within the non-Faraday potential range (1.0254 - 1.1254 V vs. RHE), scan rate changed from 10 to 100 mV s^{-1}, increased with 10 mV s^{-1} each time.

1.2.6 Assembly and testing of the Zn-air battery

As for the liquid Zn-air battery, in order to avoid electrolyte leakage, we physically compounded the SSM-based catalyst with the waterproof/breathable carbon film, and then assembled the complex as the air-cathode of the Zn-air battery. Of which, the electrode area that participating in the battery testing is 0.785 cm^2 (circular area with a radius of 0.5 cm).

Both the charge and discharge curves were measured by the CHI 760e, the power density was calculated from the data of the discharge curve. Charge-discharge curves at current density of 10 mA cm^{-2} in this work were measured by the Land battery test system.

2. DFT calculation.

All the DFT calculations are performed by the Vienna Ab initio Simulation Package (VASP) [1] with the projector augmented wave (PAW) method [2]. The exchange-functional is treated using the generalized gradient approximation (GGA) with Perdew-Burke-Ernzerhof (PBE) [3] functional. The energy cutoff for the plane wave basis expansion was set to 400 eV. Partial occupancies of the Kohn–Sham orbitals were allowed using the Gaussian smearing method and a width of 0.2 eV. The CoNi-LDH structure was built based on the bulk structure of CoNi(OH)$_2$, where the (001) surface was built. The NiCoP cluster was built with exposed (111) surface, loading on the surface of CoNi-LDH (the surface H was removed for a stable loading of CoNiP cluster). The Brillouin zone was sampled with Monkhorst mesh of 2×2×1 for the optimization for all the structures. The self-consistent calculations apply a convergence energy threshold of 10^{-5} eV, and the force convergency was set to 0.05 eV/Å. The free energy of electrochemical steps involved electron and proton transfer was calculated following the method of computational hydrogen electrode (CHE)[4].

The free energy corrections were considered at the temperature of 298 K, following:

$$\Delta G = \Delta E + \Delta G_{ZPE} + \Delta G_U - T\Delta S$$

Where ΔE, ΔG_{ZPE}, ΔG_U, and ΔS refer to the DFT calculated energy change, the correction from zero-point energy, the correction from inner energy and the correction from entropy[5], respectively. The solvent effect was considered, calculated using VASPsol, due to the stabilization of adsorbent from the H-bond network in the water for *OH and *OOH to be -0.17 eV and -0.20 eV, respectively.[6]
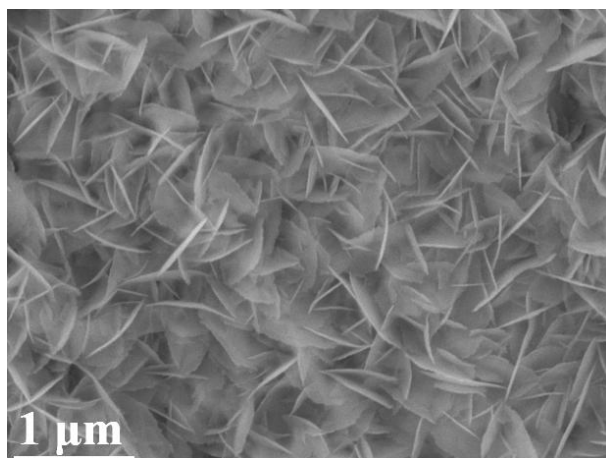
3. Supplementary Figures and Tables

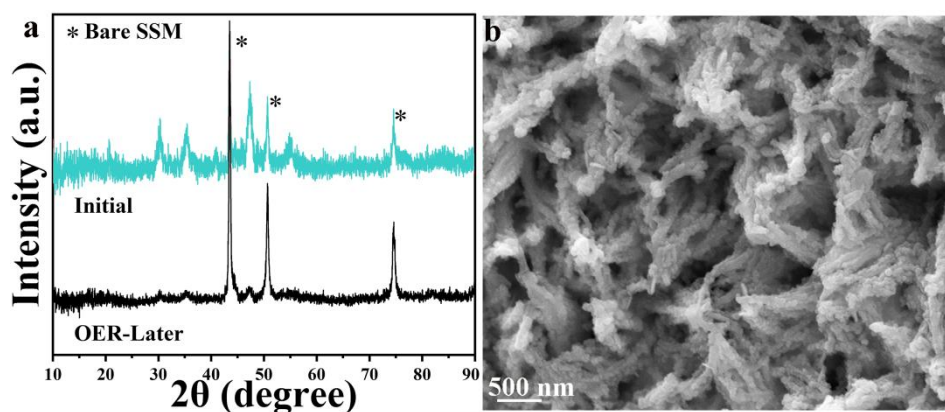**Fig. S1**. The SEM image of CoNi-LDH/SSM precursor.

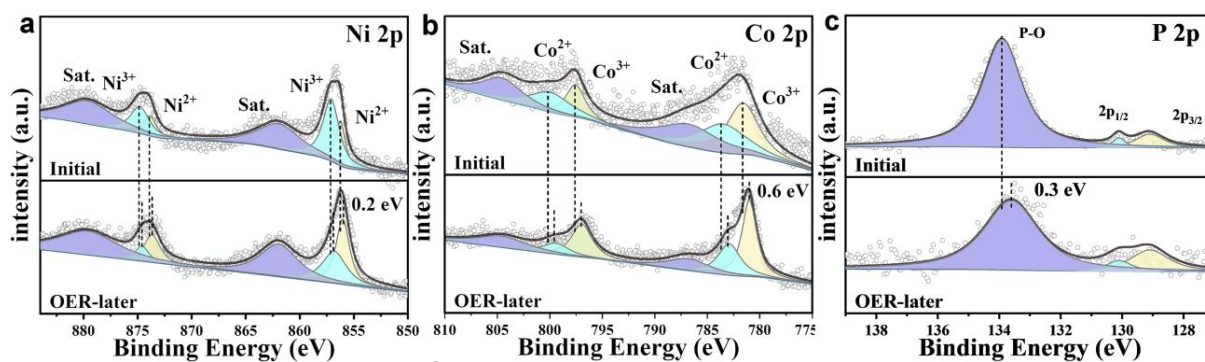**Fig. S2**. The (a) XRD and (b) SEM image of NiCoP@CoNi-LDH/SSM that OER later.

Fig. S3. The XPS results of (a) Ni 2p, (b) Co 2p and (c) P 2p in NiCoP@CoNi-LDH/SSM that the OER test later.
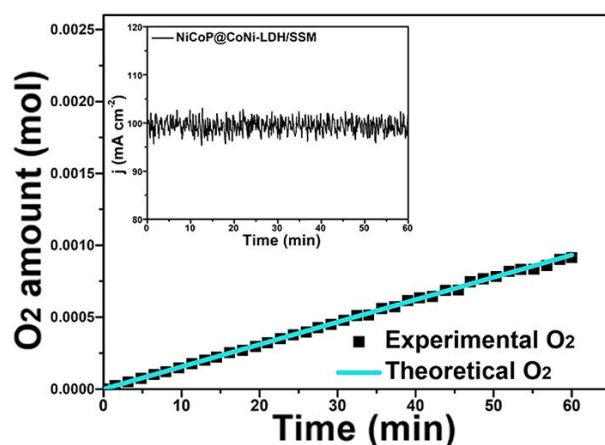
Fig. S4. The Faraday efficiency of NiCoP@CoNi-LDH/SSM for (a) OER and (b) HER, inset image is corresponding i-t curves at current density of 100 mA cm^{-2}.
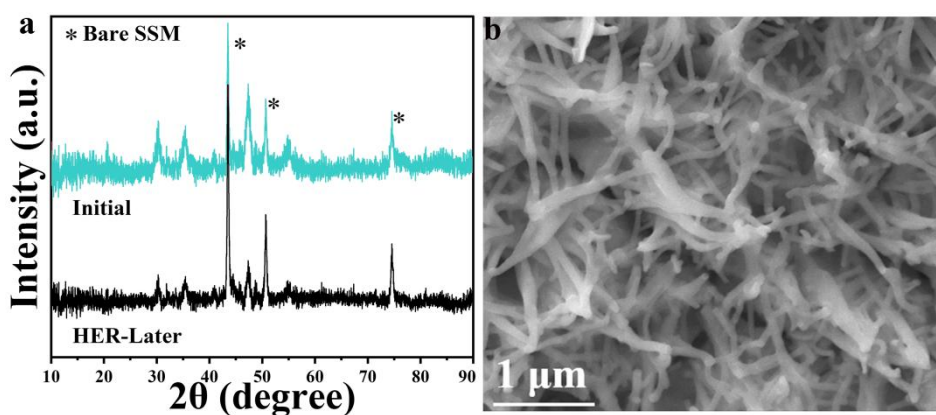

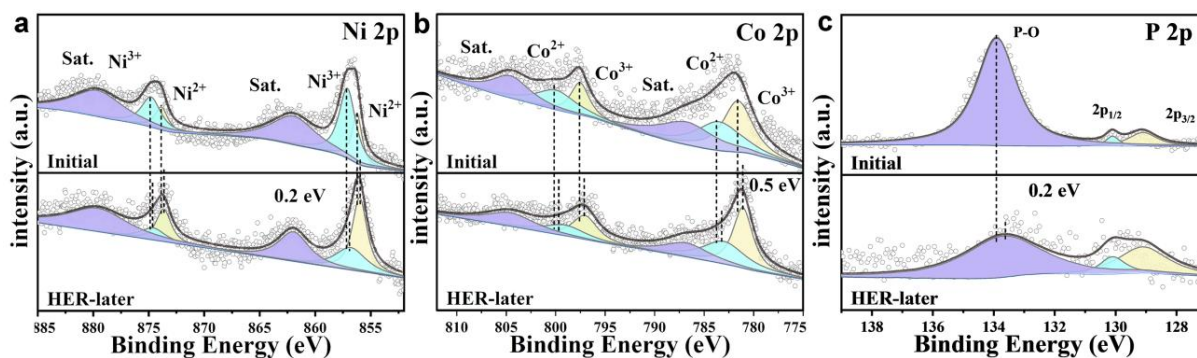**Fig. S5.** The (a) XRD and (b) SEM image of NiCoP@CoNi-LDH/SSM after the HER process.

Fig. S6. The XPS result of (a) Ni 2p, (b) Co 2p and (c) P 2p in NiCoP@CoNi-LDH/SSM that the HER test later.
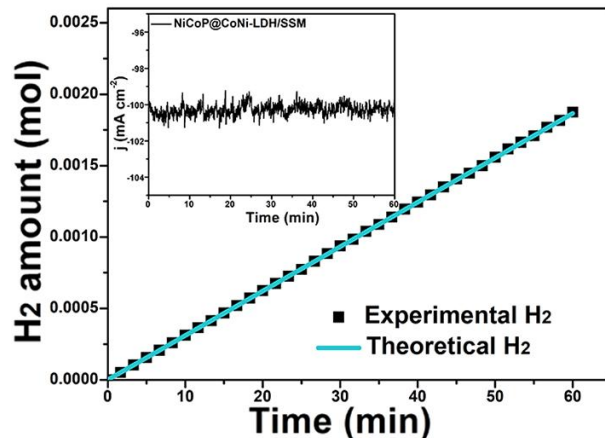
Fig. S7. The Faraday efficiency of NiCoP@CoNi-LDH/SSM for HER, inset image is corresponding i-t curves at current density of 100 mA cm^{-2}.
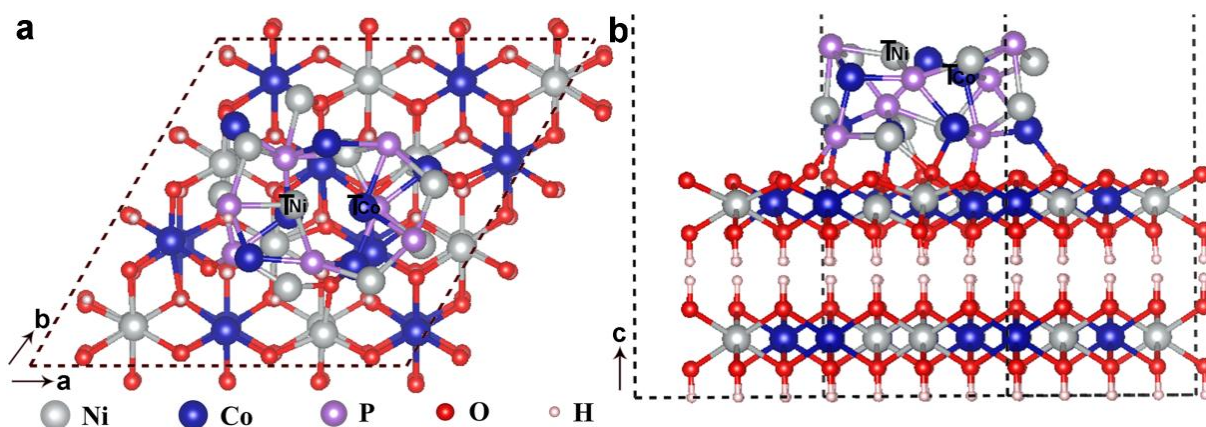

Fig. S8. (a) Top and (b) side view of the NiCoP@CoNi-LDH model, wherein, T_{Ni} and T_{Co} are the computed most active reaction sites during the HER and OER processes, respectively.
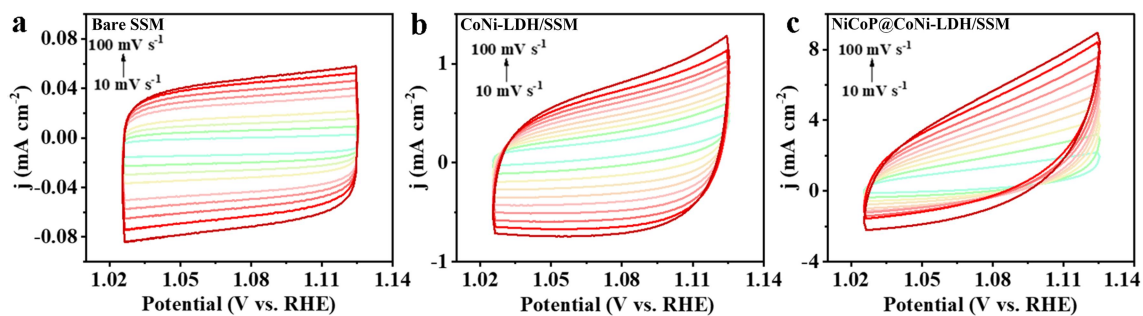

Fig. S9. The CV curves at different scan rate of (a) bare SSM, (b) CoNi-LDH/SSM, and (c) NiCoP@CoNi-LDH/SSM.

Table S1. C_{dl}, ECSA and related data of bare SSM, CoNi-LDH/SSM and NiCoP@CoNi-LDH/SSM.

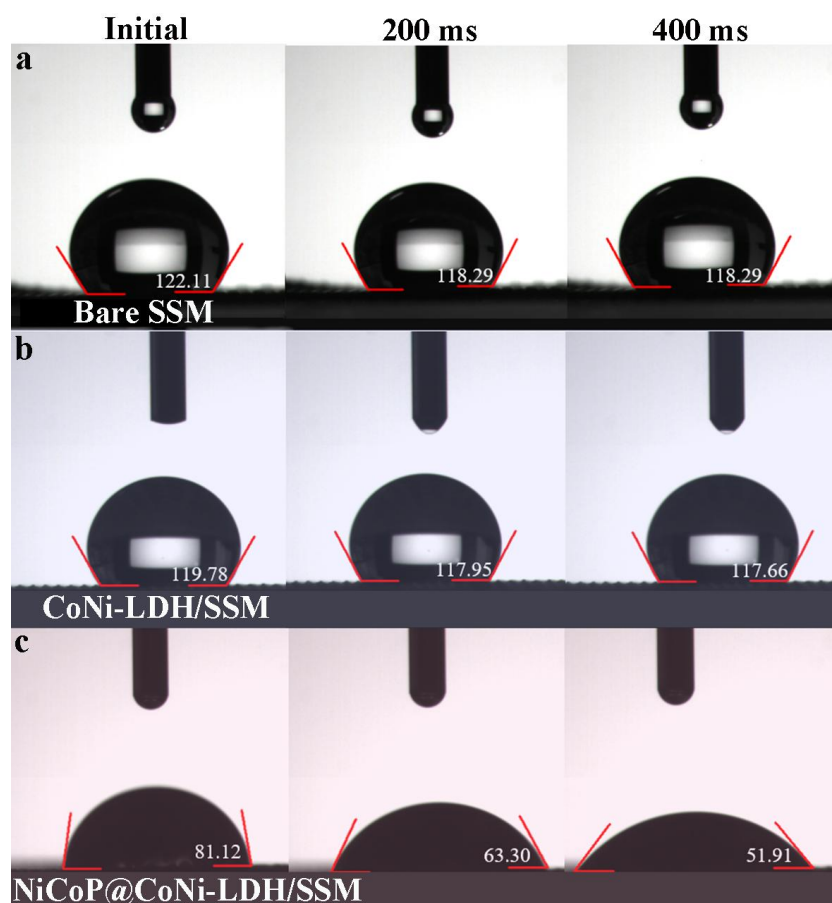| Catalyst	C_{dl} (mF cm^{-2})	C_s (mF cm^{-2})	A (cm^2)	ECSA (cm^2)
Bare SSM	0.265	0.04	0.25	1.66
CoNi-LDH/SSM	2.95	0.04	0.25	18.44
NiCoP@CoNi-LDH/SSM	21.96	0.04	0.25	137.25

Fig. S10. The water drop contact angles (CA) experiment of (a) bare SSM, (b) CoNi-LDH/SSM and (c) NiCoP@CoNi-LDH/SSM, respectively.

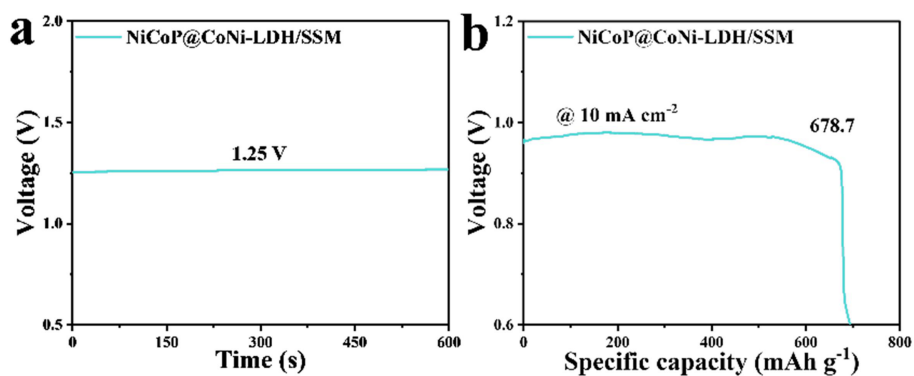**Fig. S11.** The open circuit voltage of the NiCoP@CoNi-LDH/SSM based zinc-air battery and its (b) specific capacity at current density of 10 mA cm^{-2}.
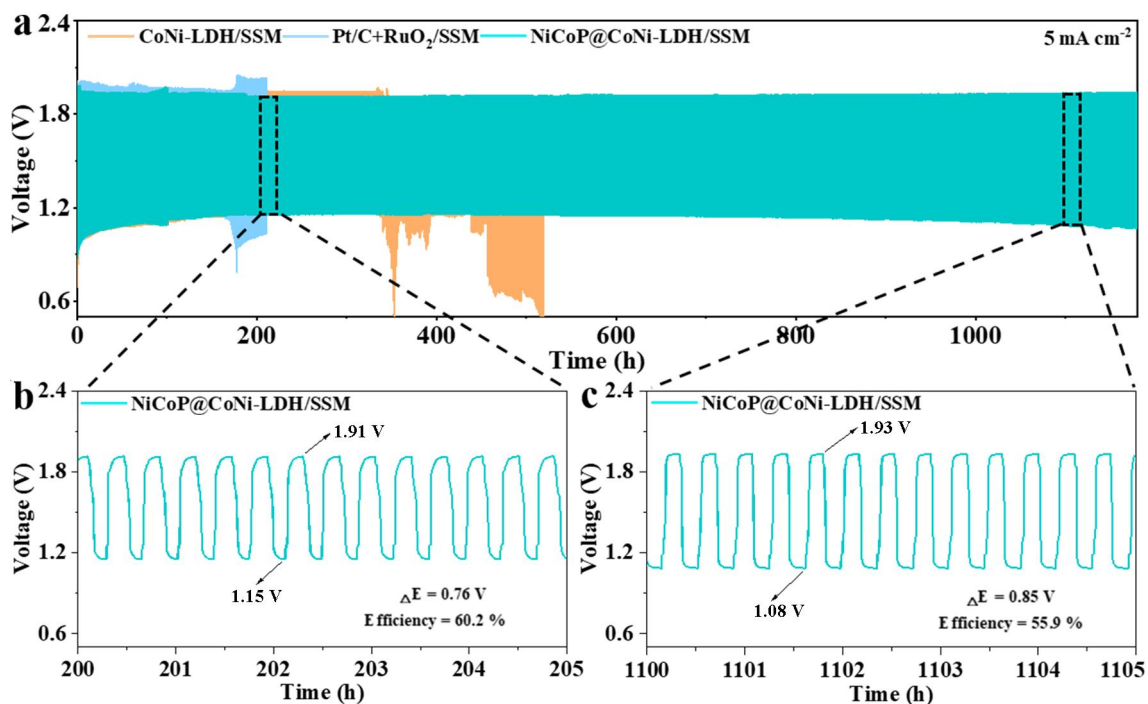

Fig. S12. (a) Galvanostatic charge-discharge cycling curves of NiCoP@CoNi-LDH/SSM, CoNi-LDH/SSM and Pt/C+RuO$_2$/SSM-based batteries at current density of 5 mA cm^{-2}. (b,c) The enlarged charge-discharge views of NiCoP@CoNi-LDH/SSM.
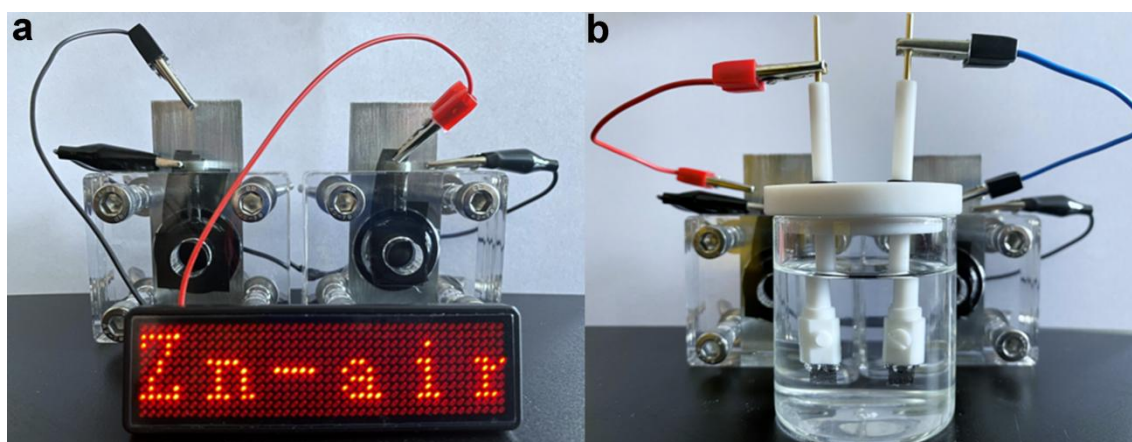
Fig. S13. (a) Lighting experiment and (b) water splitting device drived by two ZABs connected in series.

Table S2. A conclusion of the OWS, ORR and Zn-air battery activities for the recently reported self-powered trifunctional catalysts.

Trifunctional catalyst	Voltage at 10 mA cm^{-2} (OWS)	Half-wave potential (V)	Power density (mW cm^{-2})	Cycle time @ 10 mA cm^{-2} (h)	Voltage gap (V)	Reference
NiCoP@CoNi-LDH/SSM	1.579	0.89	53.4	> 1500	0.81	**This work**
CoNi-LDH/SSM	1.719	0.71	25.2	300	0.83	**This work**
Pt/C+RuO$_2$/SSM	1.626	--	44.2	160	0.84	**This work**
Pt/C/SSM	--	0.90	--	--	--	**This work**
Pt@Fe-MOF	1.46	0.84	104	95	--	*Small* 2023, 2305201
NiCoP/NiO	1.71	0.59	84.5	113	0.84--0.86	*Green Energy Environ.* 2023, 8, 601
Fe-NiCoP	1.60	--	--	900 cycles @ 5 mA cm^{-2}	--	*CrystEngComm* 2021, 23, 3861
Fe Doped MOF CoV@CoO nanoflakes	1.53	0.75	138	50	0.89	*Nano Energy*, 2021, 106238
Co-MOF-800	--	0.84	144	85 @ 1 mA cm^{-2}	0.46--0.58	*J. Energy Chem.* 2021, 56, 290
Co@NCL	1.70	0.84	170	200	0.88	*Chem. Eng. J.*, 2021, 423, 130313
Co/N-CNF-800	1.80	0.86	--	50	1.39	*ACS Appl. Mater.*

						Interfaces 2022, 14, 4399
Fe-Co-Ni MOF	1.60	0.75	161	120 @ 5 mA cm^{-2}	0.46--0.56	*J. Am. Chem. Soc.* 2022, 144, 15903
3%IrO$_x$/NCNT	1.52	0.75	59.3	120 @ 5 mA cm^{-2}	0.65	*Electrochimica Acta* 2021, 380, 138215
CoFe@NC/NCHNSs-700	1.66	0.92	184	50	~0.87	*Appl. Catal., B* 2021, 298, 120512
CoDNG900	--	0.86	205.6	667	0.82	*Appl. Catal., B* 2021, 281, 119514
Pt/d-CoP/NPC	1.53	0.82	182.8	200	~1.05	*Chinese J. Catal.* 2023, 46, 36
MoCoP-NPC	1.65	0.88	175.2	300	0.47--0.5	*Small* 2023, 2302414
FeZn$_4$Co@CNFs	--	0.84	107.6	118	~0.87	*J. Power Sources* 2022, 521, 230925
Co-COP	--	0.80	83.6	--	--	*Catal. Sci. Technol.* 2023, 13, 6321
SC-Cu$_{SA}$-NC	1.58	0.83	124.9	120	~0.9	Composites Part B 2023, 253, 110575
Fe-N-C/FeP$_x$/NPSC	1.57	0.90	216.9	93	0.87-0.96	*Chem. Eng. J.* 2021, 421, 129704
RuCoO$_x$	1.54	0.85	160	1100 cycles @ 5 mA cm^{-2}	~0.86	*Nano Lett.* 2021, 21, 9633
RuCo/NPC	1.68	0.80	79.4	16.67 @ 2 mA cm^{-2}	~0.75	*Chem. Commun.* 2021, 57, 1498
Re-Ni$_3$S$_2$/NG/NF	1.58	0.66	99	266	~0.88	*Composites Part B* 2022, 234, 109670
NAC@Co$_3$O$_4$/NCNTs/CNF	--	0.83	267.6	67	0.8--1.25	*Inorg. Chem. Front.* 2022, 9, 2517
Pd-coated (CoFe/NCNTs)	1.60	0.82	261	50	0.69	*Green Energy Environ.* 2022, 7, 933
CoP/Co$_3$O$_4$-fC-pPVP	1.58	0.84	154	727 @ 5 mA cm^{-2}	~0.75	*Electrochimica Acta* 2022, 412, 140134

CoFeN-NCNTs//CCM	1.63	0.84	145	445	0.76	*Adv. Funct. Mater.* 2021, 2107608
B-CoSe$_2$@CoNi LDH HNA	1.58	0.81	181.5	70 @ 1 mA cm^{-2}	~0.8	*Adv. Sci.* 2022, 2104522
NiCu-MoS$_2$	1.62	0.85	283	133	0.71-0.74	*J. Mater. Chem. A* 2023, 11, 18336
FeSn$_2$@FeSnO$_x$@S-N-C-900	--	0.88	64.5	24	1.5	*Electrochimica Acta* 2019, 320
SnSb-NC	--	0.87	195.8	1106	~1.3	*Inorg. Chem. Front.* 2023, 10, 3568
Sn$_{x=0.15}$-Ga$_2$O$_3$	--	0.70	138	30	0.58	*Small* 2022, 18, 2202648

4. Reference

[1] Kresse, G.; Furthmüller, J., Efficiency of ab-initio total energy calculations for metals and semiconductors using a plane-wave basis set. *Comp. Mater. Sci.* **1996**, 6 (1), 15-50..

[2] Blochl, P. E., Projector augmented-wave method. *Phys. Rev. B, Condens. Matter* **1994**, 50 (24), 17953-17979.

[3] Perdew, J. P.; Chevary, J. A.; Vosko, S. H.; Jackson, K. A.; Pederson, M. R.; Singh, D. J.; Fiolhais, C., Atoms, molecules, solids, and surfaces: Applications of the generalized gradient approximation for exchange and correlation. *Phys. Rev. B, Condens. Matter* **1992**, 46 (11), 6671-6687.

[4] Nørskov, J. K.; Rossmeisl, J.; Logadottir, A.; Lindqvist, L.; Kitchin, J. R.; Bligaard, T.; Jónsson, H., Origin of the Overpotential for Oxygen Reduction at a Fuel-Cell Cathode. *The J. Phys. Chem. B* **2004**, 108 (46), 17886-17892.

[5] Guo, C.; Tian, X.; Fu, X.; Qin, G.; Long, J.; Li, H.; Jing, H.; Zhou, Y.; Xiao, J., Computational Design of Spinel Oxides through Coverage-Dependent Screening on the Reaction Phase Diagram. *ACS Catal*. **2022**, 12 (11), 6781-6793.

[6] Guo, C.; Fu, X.; Xiao, J., Theoretical Insights on the Synergy and Competition between Thermochemical and Electrochemical Steps in Oxygen Electroreduction. *The J. Phys.Chem. C* **2020**, 124 (47), 25796-25804.